scientific reports

Check for updates

OPEN

Deficiency in NPC2 results in disruption of mitochondria-late endosome/lysosomes contact sites and endo-lysosomal lipid dyshomeostasis

Raffaele Pastore[1,3], Lihang Yao[2], Nathan Hatcher[2], Martin Helley[1], Janet Brownlees[1] & Radha Desai[1]✉

Dysfunction of the endo-lysosomal intracellular Cholesterol transporter 2 protein (NPC2) leads to the onset of Niemann–Pick Disease Type C (NPC), a lysosomal storage disorder. Metabolic and homeostatic mechanisms are disrupted in lysosomal storage disorders (LSDs) hence we characterized a cellular model of NPC2 knock out, to assess alterations in organellar function and inter-organellar crosstalk between mitochondria and lysosomes. We performed characterization of lipid alterations and confirmed altered lysosomal morphology, but no overt changes in oxidative stress markers. Using several techniques, we demonstrated that contacts between mitochondria and late endosomes/lysosomes are reduced in NPC2$^{-/-}$ HEK cells, we observed that the acidic compartments are swollen and lipid dense. Quantification of endogenous lipids in HEKNPC2$^{-/-}$ cells by mass spectrometry reveals accumulation of lipid species indicative of sphingolipid metabolic dysregulation within the lysosome. Specifically, HEK NPC2$^{-/-}$ cells exhibit marked elevation of glucosylsphingosine and glucosylceramides, substrates of beta glucocerebroside (GBA), as well as accumulation of sphingosine and sphingomyelins. Our studies suggest an involvement of NPC2 in the formation of contact sites between mitochondria and lysosomes and support the hypothesis of a role for NPC2 in the endo-lysosomal trafficking pathway and dynamic organellar crosstalk.

NPC (Niemann–Pick Type C) disease is an autosomal recessive lysosomal storage disorder caused by mutations in either the *NPC1* or *NPC2* genes. Both variations of the NPC disease are biochemically and clinically identical, manifesting as progressive neurodegenerative diseases[1–3]. Deficits in the NPC1 protein have been associated with alterations in mitochondria-ER and mitochondria-late endosomes/lysosome membrane contact sites (MCS)[3,4]. For example, in 2019 Hoeglinger and colleagues demonstrated that the extent of contact between late endosomes/lysosomes and the ER was decreased, whereas it was increased between mitochondria and late endosome/lysosomes in cellular models deficient in NPC type 1[4]. NPC2 has been linked to NPC1-independent clearance of unesterified cholesterol from lysosomes[5,6]. Upon malfunction of either NPC1 or NPC2 proteins, cholesterol and sphingolipids accumulate within late endosomes/lysosomes leading to the onset of the Niemann–Pick C disease (NPC) type 1 and type 2, respectively. Here, we focused on establishing whether NPC2 is involved in the formation of MCS between mitochondria and late endosome/lysosomes. Inter-organelle membrane contact sites are transient structures that form when the membranes of two organelles are in proximity (10–80 nm), tethered by protein–protein or protein-lipid interactions. Instead of fusing with each other the two organelles form a dynamic platform with a specific function (e.g. exchange of ions and metabolites) which is able to influence the homeostasis of the cell[7–9]. Formation of mitochondria-late endosomes/lysosomes MCS is promoted by GTP-Rab7a, a GTPase localised on the lysosomal surface, through its effector proteins which constitute the actual tether between the membranes of the two organelles. However, the composition of this GTP-Rab7a regulated junction is still unknown[10,11]. Several proteins associated with the formation of mitochondrial-late endosomal/lysosomal contact sites have been associated with human disease[4,12–14]. Untethering of mitochondria-late endosomes/lysosomes MCS occurs when TBC1D15, a Rab7 GTPase activating protein (GAP), is recruited to

[1]MSD R&D Innovation Centre, 120 Moorgate, London EC2M 6UR, UK. [2]Merck Research Laboratories, Merck & Co., Rahway, NJ, USA. [3]Department of Medicine and Health Sciences 'Vincenzo Tiberio', University of Molise, via F. De Santis, 86100 Campobasso, Italy. ✉email: radha.desai@msd.com

mitochondria by Fis1 and drives the hydrolysis of GTP-Rab7a, turning the GTPase into its inactive and cytosolic form GDP-Rab7a[11,15,16]. Contact sites between mitochondria and lysosomes can serve as signalling platforms with functional consequences for both mitochondrial and lysosomal function. Mitochondrial lysosomal MCS have been implicated in intraorganellar Ca^{2+} homeostasis via TRPML1[8,11,17] lipid homeostasis and cholesterol import into mitochondria[5,18–20]

The soluble NPC2 protein transports unesterified cholesterol from the inner lumen to the limiting membrane for subsequent clearance by secretion[21]. The mechanism through which unesterified cholesterol is cleared from lysosomes is not clearly understood. It has been hypothesised that the egress of cholesterol from lysosomes involves two possible routes- an NPC1-dependent pathway, where NPC1 mediates the transport of free cholesterol across the limiting lysosomal membrane, or, an NPC1 independent pathway[5,6,19,22,23] NPC2 is able to directly interact with lipid membranes, catalyse cholesterol transfer between them and promote intermembrane interaction[24,25]

We hypothesized that NPC2 may play a role in the formation of mitochondrial lysosomal MCS to facilitate cholesterol egress. We used a *NPC2* knockout HEK cell line to characterise the lipid dyshomeostasis and then proceeded to interrogate whether this organellar contact mechanism is disrupted because of NPC2 deficiency. We used ultrastructural electron microscopy imaging to confirm direct interaction between the organelles, dSTORM super resolution immunofluorescence to visualize molecular proximity between outer membrane proteins (TOM20—mitochondria, LAMP1—lysosome), and proximity ligation assay to quantify MCS in WT and *NPC2*$^{-/-}$ HEK cells. Furthermore, we were able to confirm significant lipid dys-homeostasis in the *NPC2*$^{-/-}$ HEK cells using mass-spec analysis and cholesterol accumulation using filipin staining. The reintroduction of the NPC2 protein was able to significantly reduce cholesterol accumulation in lysosomes. This study highlights a role for NPC2 in mitochondrial-lysosomal MCS, and raises the possibility of an egress route, while also confirming that mitochondrial function is maintained when there is disruption of these contact sites.

Results

We used the mutant *NPC2*$^{-/-}$ HEK cell line as a model of the Niemann–Pick-C disease type 2. First, we characterized the *NPC2*$^{-/-}$ HEK to assess whether it recapitulates the cellular hallmarks of NPC2 disease.

Late endosomes/lysosomes of *NPC2*$^{-/-}$ HEKs are enlarged and exhibit dense filipin staining

By immunofluorescence we analysed the mitochondrial and late endosomal/lysosomal network morphology in WT HEK and *NPC2*$^{-/-}$ HEK cells. To this end, the two cell lines were co-stained with antibodies against LAMP1 and TOM20 to label the late endosomal/lysosomal and outer mitochondrial membranes respectively. Super resolution microscopy dSTORM shows that in the *NPC2*$^{-/-}$ HEKs the morphology of mitochondria is unaltered whereas late endosomes/lysosomes appear enlarged and rounded in comparison to the late endosomes/lysosomes of the WT HEK. (Fig. 1a). This observation was confirmed by Transmission Electron Microscopy (TEM), Figs. 1b, 3c. TEM data shows that late endosomes/lysosomes of the *NPC2*$^{-/-}$ HEKs are twice the size of the late endosome/lysosomes in the healthy control, with their lumen containing multiple vesicles that are coalesced together and dense.

In order to investigate the composition of the lipids stored within late endosomes/lysosomes of the *NPC2* mutant cells, we co-stained WT HEK and *NPC2*$^{-/-}$ HEKs with an antibody to LAMP1, to visualize the lysosomal network, and with filipin, a fluorescent probe that selectively binds unesterified cholesterol[26]. Fluorescent microscopy images of Fig. 2a demonstrate that late endosomes/lysosomes of the *NPC2*$^{-/-}$ HEK cells contain higher amounts of unesterified cholesterol. We observe that the LAMP1 signal surrounds the filipin signal forming green circles (late endosomes/lysosomes) around a blue signal (unesterified cholesterol). In addition, using high content quantification of the filipin fluorescence intensity we confirmed that the levels of unesterified cholesterol in the *NPC2*$^{-/-}$ HEKs are increased in comparison to the WT control (Fig. 2b). Interestingly, treatment of the *NPC2*$^{-/-}$ HEKs with cholesterol mobilizer HP-β-cyclodextrin[27] clears the cells of unesterified cholesterol and reduces the size of late endosomes/lysosomes that is reverted back to the same size and shape observed in the healthy control (Fig. 2a). The HP-β-cyclodextrin data establish a link between the increased size of lysosomes in the *NPC2*$^{-/-}$ HEKs and the accumulation of lipids in their lumen.

Quantification of cellular sphingolipid species by targeted mass spectrometry (here we discuss the statistics of 10 technical replicates, which are observed consistently across biological replicates) revealed elevated concentrations of sphingosine (Fig. 2c), glucosylsphingosine (Fig. 2d), glucosylceramides (Fig. 2e) and sphingomyelins (Fig. 2f), but not ceramide species in the *NPC2*$^{-/-}$ HEK cells compared to WT HEK controls (Fig. 2g). The elevated sphingolipid species observed here suggest that loss of NPC2 function results in deficits in lysosomal salvage catabolic pathways resulting in accumulation of glycosphingolipid and sphingomyelin intermediates downstream of abundant ceramide precursors.

Deficiency of the NPC2 protein leads to reduced mitochondrial-lysosomal contact sites

Next, we investigated the organellar contact sites between mitochondria and late endosomes/lysosomes in the WT HEK and *NPC2*$^{-/-}$ HEK, by optimising a Proximity Ligation Assay with antibodies against lysosomal protein LAMP1 and the outer mitochondrial membrane protein TOM20. Detection of the TOM20-LAMP1 PLA signal spot area per cell and of the cytoplasmic TOM20-LAMP1 PLA signal intensity showed that contacts between the membranes of mitochondria and late endosomes/lysosomes in the in the *NPC2*$^{-/-}$ HEKs were reduced in comparison to WT HEKs (Fig. 3a Supp. Figure 1c). In addition, qualitative analysis of several representative electron micrographs and of the zooms of their insets confirm what we observed by Proximity Ligation Assay, that in the *NPC2*$^{-/-}$ HEK cells the number of contacts between mitochondria and lysosomes is decreased in comparison to the matched control (Fig. 3b). In addition, high content quantification of the LAMP1 spot area shows that the size of late endosomes/lysosomes in the *NPC2*$^{-/-}$ HEKs is double the size of the late endosomes/

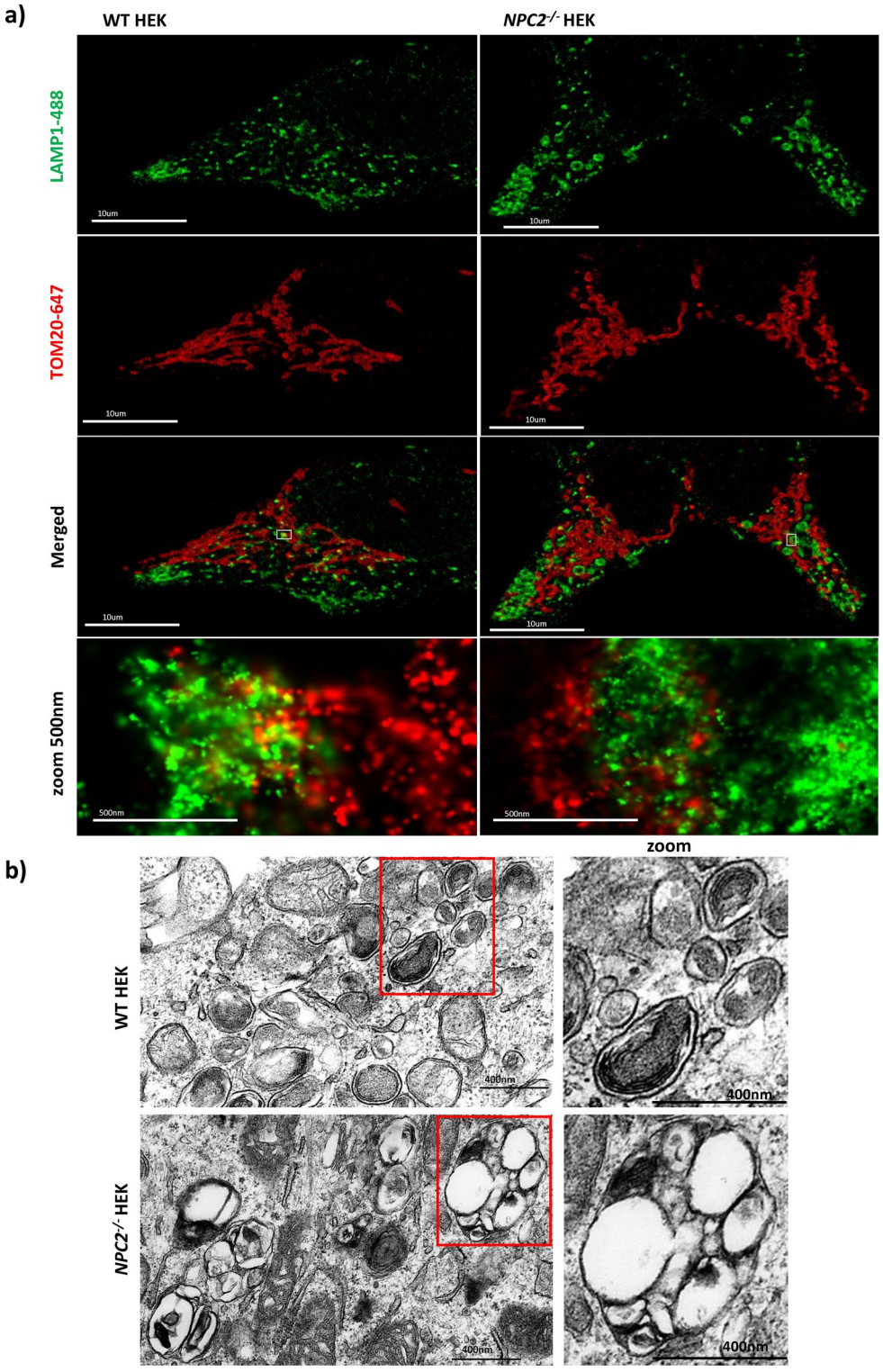

Fig. 1. Morphology of late endosomes/lysosomes in WT and *NPC2*$^{-/-}$ HEK cell lines. **a** dSTORM (direct Stochastic Optical Reconstruction Microscopy) images of 4% PFA fixed WT and *NPC2*$^{-/-}$ HEK cells co-stained with antibodies against endogenous TOM20 (red; outer mitochondrial membrane) and LAMP1 (green; lysosomal membrane). Images were acquired with the ONI microscope. For each cell line, WT HEK and *NPC2*$^{-/-}$ HEK, the mitochondrial and late endosomal/lysosomal networks are represented. Scale bar = 10 µm. The insets (bottom row) show contact sites between the lysosomal and the outer mitochondrial membranes with more overlap in the WT cells. Scale bar = 500 nm. **b** TEM representative images of late endosomes/lysosomes in WT HEK (top row) and *NPC2*$^{-/-}$ HEK (bottom row). Scale bar = 400 nm.

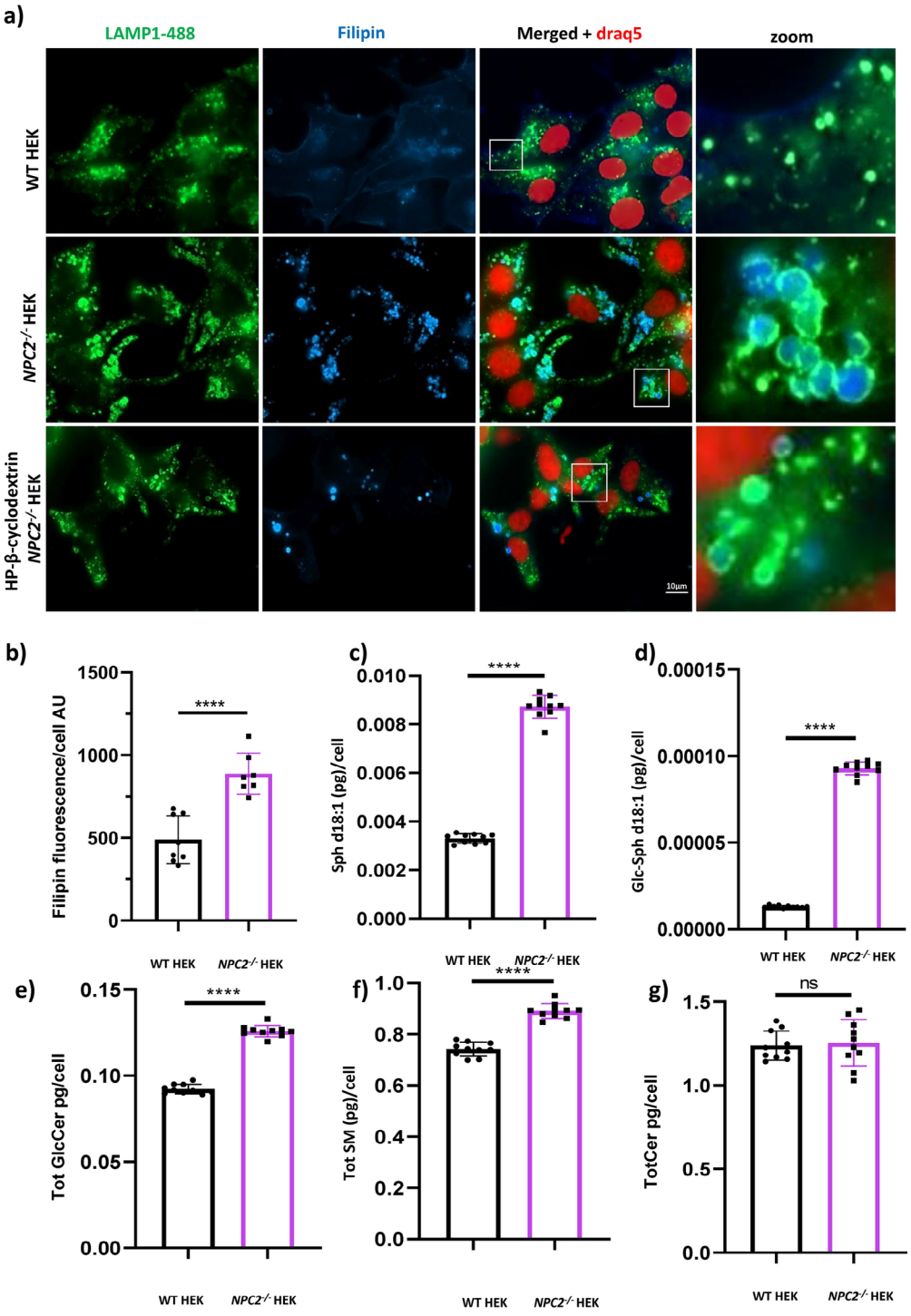

Fig. 2. Lipid dyshomeostasis in NPC2$^{-/-}$ HEKs. **a** Representative epifluorescence images of untreated WT HEKs, NPC2$^{-/-}$ HEKs and HP-β-cyclodextrin treated NPC2$^{-/-}$ HEKs, labelled with the fluorescent probe filipin (blue) to mark free cholesterol, DRAQ5-647 (red) to stain the nucleus and an antibody to LAMP1 to mark the late endosomal/lysosomal membrane (green). Insets (bottom row) show late endosomes of the NPC2$^{-/-}$ HEKs co-stained with LAMP1 and filipin (unesterified cholesterol) whereas no filipin is detectable in late endosomes of WT HEK. **b** Quantification of the filipin fluorescence intensity (unesterified cholesterol) detected in WT andNPC2$^{-/-}$ HEKs. AU = arbitrary units **c**–**g** Mass spectrometry quantitation of the levels of: **c** Sphingosine (Sph d18:1); **d** Glucosylsphingosine (GlcSph d18:1); **e** Total Glucosylceramide (sum of GlcCer chain length species d16:0, d18:0, d20:0, d22:0, d24:0, d24:1); **f** Total Sphingomyelin (sum of SM chain length species d16:0, d18:0, d20:0, d22:0, d24:0, d24:1) and **g** Total Ceramide (sum of Cer chain length species d16:0, d18:0, d20:0, d22:0, d24:0, d24:1) in WT and NPC2$^{-/-}$ HEKs. Mass- spec data are reported as pg/cell and expressed as mean +/- standard deviation (SD). $^{****}p < 0.0001$; $^{**}p < 0.01$; ns = not significant. *p* values were calculated with the Student's T test. Each dot of the graphs indicates a technical replicate (10) replicates used.

lysosomes in the healthy control (Fig. 3d,e). Furthermore, in both the EM images (Fig. 3c) as well as dSTORM visualisation (Fig. 1a), we are also able to observe the phenomenological formation of mitochondrial-lysosomal contact sites, without any other membrane structures between the two organelles. Hence, we interpret that the observed quantification by PLA is representative of the proximity between the organelles rather than autophagy of the organelle. Using multiple microscopy techniques, enables a more systematic study of MCS (Suppl Fig. 1)—(i) the PLA signal marks individual contact site formation within a distance of 80 nm[28,29] (ii) EM provides a visual confirmation of the mitochondrial-lysosomal contact site rather than autophagy of mitochondria (iii) dSTORM super resolution microscopy confirms the overlapping signals of the antibodies and confirms selectivity of the primary antibodies we use for PLA. These consolidated data indicate that in the *NPC2*$^{-/-}$ HEK cells the contacts between mitochondria and late endosomes/lysosomes are reduced, despite an increase in the cell volume occupancy of the late endosomal/lysosomal organelles.

NPC2$^{-/-}$ deficiency does not disrupt mitochondrial respiratory function but results in subtle hyper polarization mitochondrial membrane potential

As a next step, to understand if mitochondrial health was compromised by the absence of the NPC2 protein, we measured the mitochondrial membrane potential, the oxygen consumption rate (OCR) and the cellular area occupied by the mitochondrial network in both the *NPC2*$^{-/-}$ HEK and control HEK cells. A TMRM assay was performed by flow cytometry to measure the mitochondrial membrane potential in WT HEK and *NPC2*$^{-/-}$ HEK cell lines. The increase in the TMRM fluorescence intensity detected in the *NPC2*$^{-/-}$ HEK compared with the WT HEK indicated hyperpolarisation (Fig. 4a,c). Treatment of WT HEK and *NPC2*$^{-/-}$ HEK cells with the mitochondrial uncoupler carbonyl cyanide-m-chlorophenylhydrazone (CCCP) was used as a TMRM assay control. As expected, CCCP induced depolarization of mitochondria in both cell lines, as shown by the decreased intensity of the TMRM signal (Fig. 4b).

A Seahorse mito-stress test was performed to measure the oxygen consumption rate (OCR) in both WT HEK and *NPC2*$^{-/-}$ HEK cells and ETC function. As shown in Fig. 4d, there was no difference in the OCR between the two cell lines neither under basal condition nor after the sequential treatment of the cells with stressors of the Electron Transport Chain (oligomycin, carbonylcyanide-p-trifluoromethoxy phenylhydrazone (FCCP), rotenone and antimycin), thus supporting the observation of only subtle changes in mitochondrial physiology.

Immunofluorescence with an antibody against TOM20 showed that the cytoplasmic area occupied by the mitochondrial network as well as the shape of the mitochondria appear similar in both cell types (Fig. 4e,f). Western blot showed that the expression levels of TOM20 are the same in both cell lines, corroborating the finding in immunofluorescence (Fig. 4g). In addition, EM images confirmed intact mitochondria and cristae architecture. Overall data therefore suggest that despite an increased mitochondrial membrane potential, mitochondria of the *NPC2*$^{-/-}$ HEK cells are like the WT control cells. We also tested whether there is increased oxidative stress or oxidative stress response to mitochondrial toxins (Rotenone) in NPC2 deficient cells (Supp. Fig. 4). We also confirmed through western blot (Fig. 4h) that while the LAMP1 protein is higher in the mutant cell line due to lysosomal accumulation, the mitochondrial mass (as measured by TOM20 protein) is like wild type.

Reconstitution of the NPC2 protein rescues the lysosomal enlargement and cholesterol accumulation in *NPC2*$^{-/-}$ HEK cell line

To demonstrate that the pathological phenotypes observed in the *NPC2*$^{-/-}$ HEK cell line are a direct consequence of the lack of the NPC2 protein, we ectopically expressed NPC2 into the *NPC2*$^{-/-}$ HEK cells. For this purpose, *NPC2*$^{-/-}$ HEK cells were transduced with either a lentiviral vector encoding *NPC2* or with a lentiviral control vector. The cells were fixed and co-stained with an antibody against LAMP1 and with filipin, the fluorescent marker of unesterified cholesterol. Reconstitution of the NPC2 protein was able to revert enlargement of lysosomes, increased expression of LAMP1 and build-up of free cholesterol back to normal (Fig. 5a–c). Indeed, the *NPC2*$^{-/-}$ HEK cells expressing the recombinant NPC2 protein are indistinguishable from the WT HEK cells (Fig. 5a). High content quantification of the LAMP1 and filipin cytoplasmic intensity confirm reduction of both the expression of LAMP1 and of the levels of unesterified cholesterol in the lenti-h*NPC2* transduced *NPC2*$^{-/-}$ HEK cells in comparison to control (Fig. 5b,c).

Discussion

In this study, we investigate the contact sites between mitochondria and late endosome/lysosomes in a cellular model of the Niemann–Pick-C type-2, a lysosomal storage disorder also classified as a progressive neurodegenerative disease[30]. Membrane contact sites are transient cellular platforms for the exchange of ions and metabolites among organelles which, when dysregulated, may contribute to pathological deficits in homeostasis, observed in several diseases[12,31,32]. It has been hypothesised that delivery of cholesterol to mitochondria partly occurs at MCS with ER and lysosomes[20,33]. Kennedy and colleagues demonstrated that depletion of the NPC2 protein in CHO cells with functional NPC1 transmembrane protein presented lower levels of mitochondrial cholesterol[5]. This finding raised the possibility of a role for the NPC2 protein in the formation of MCS between mitochondria and late endosomes/lysosomes, which we have explored in this study. Characterisation of the *NPC2*$^{-/-}$ HEK cells showed that the morphology of their lysosomal network, monitored by IF LAMP1 staining, is completely altered, with late endosomes/lysosomes that are swollen and rounded in comparison to WT HEK cells. In addition, TEM, filipin staining of unesterified cholesterol and mass spec lipid profiling revealed that the enlarged lysosomes of the *NPC2*$^{-/-}$ HEK cells are full of lipids. The immunofluorescence LAMP1-filipin co-staining of WT HEK and *NPC2*$^{-/-}$ HEK cells clearly showed that unesterified cholesterol accumulates within the late endosomes/lysosomes of the *NPC2*$^{-/-}$ HEK cells. Moreover, mass spectrometry analysis of several sphingolipid species in WT HEK and *NPC2*$^{-/-}$ HEK cells showed that the levels of sphingosine,

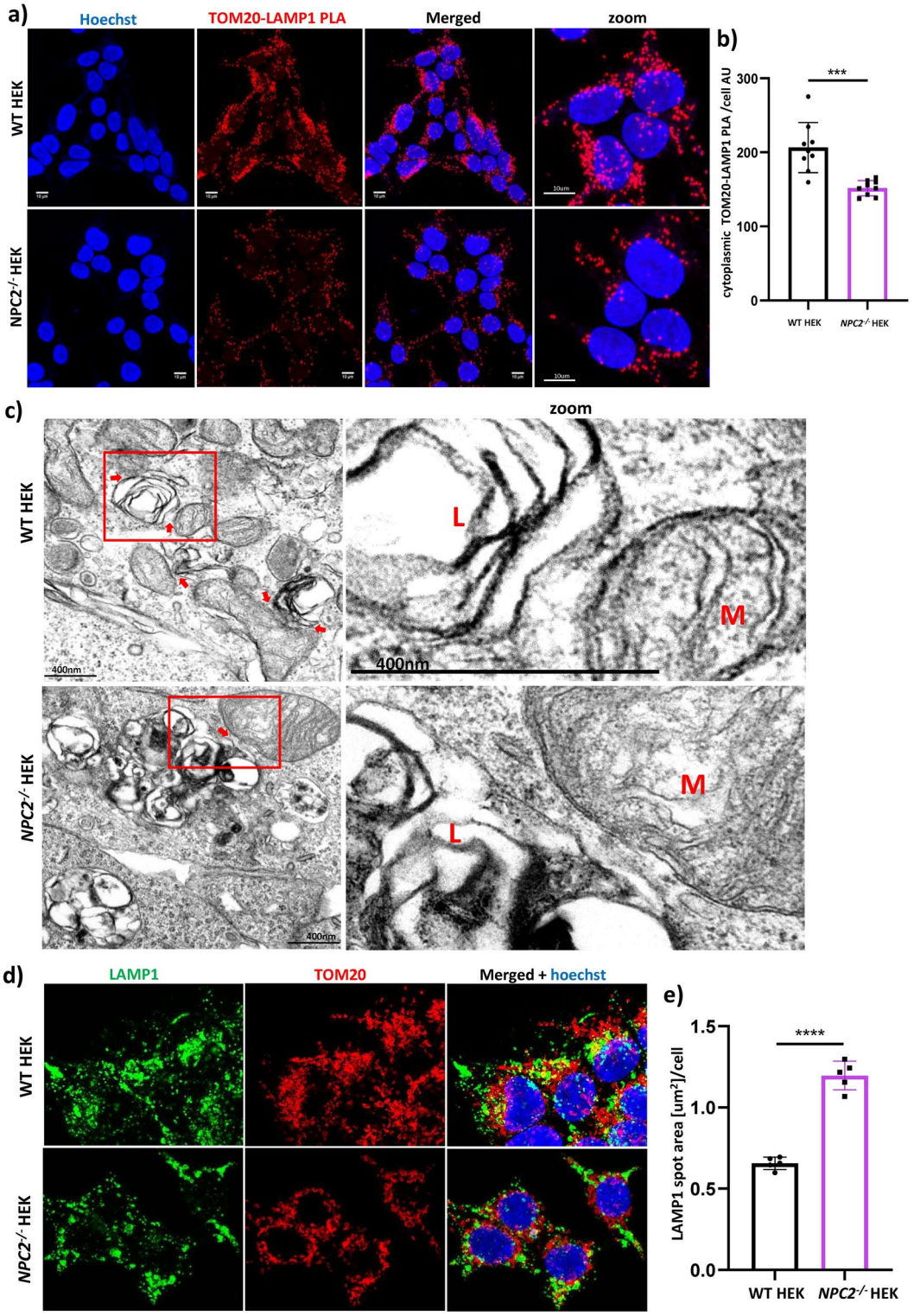

glucosylsphingosine, total sphingomyelin and total glucosylceramide are significantly elevated in the *NPC2*$^{-/-}$ HEK cells in comparison to the WT HEK cells. In fact, EM images showed that vesicles carrying lipids are only visible within the perimeter of the late endosomal/lysosomal membrane and not elsewhere in the cytoplasm of the *NPC2*$^{-/-}$ HEK cells, similar to previous observations[33]. Using a chemically modified sphingosine analogue, the photoactivable and clickable sphingosine, it was shown that in NPC1-deficient fibroblasts, sphingosine accumulates in late endosomes/lysosomes[33]. Here we show that increased levels of glucosylsphingosine are detected in a cellular model of the Niemann–Pick C disease type-2 similar to a blood diagnostic hallmark of the lysosomal storage disorder Gaucher disease (GD)[34,35]

Unlike the changes observed in the lysosomal network, the biology of mitochondria in the *NPC2*$^{-/-}$ HEK cells do not appear to be severely altered. In fact, even though the TMRM assay shows that mitochondria of the *NPC2*$^{-/-}$ HEK cells are hyperpolarised, this increase in the mitochondrial membrane potential is not

◀**Fig. 3**. Study of the membrane contact sites between mitochondria and late endosomes/lysosomes in WT HEK and *NPC2*$^{-/-}$ HEK. **a** representative confocal images of fluorescent Proximity Ligation Assay (PLA) performed on WT HEK and *NPC2*$^{-/-}$ HEK cells labelled with primary antibodies against LAMP1 (late endosomes/lysosomes) and TOM20 (outer mitochondrial membrane). Red dots = fluorescent TOM20-LAMP1 PLA signal membrane contact sites between mitochondria and lysosomes. Nuclei were stained with Hoechst (blue). Scale bar = 10 µm. **b** High content analysis of the cytoplasmic TOM20-LAMP1 PLA signal intensity detected in WT HEK and *NPC2*$^{-/-}$ HEK. AU = arbitrary units. Data are expressed as mean per well (each dot of the bar graph indicates one well of a 96 well plate) + /- SD. ****$p < 0.0001$. p value was calculated with the Student's T test. **c** Transmission Electron microscopy (TEM) panel displaying representative micrographs of WT HEK and *NPC2*$^{-/-}$ HEK cells. L = late endosome/lysosome; M = mitochondrion; scale bar = 400 nm. Micrographs' insets (right column) depict contact sites between the outer mitochondrial and the lysosomal membranes in both cell lines. MCSs = membrane contact sites; mito-lyso (mitochondria-late endosomes/lysosomes). **d** Confocal microscopy images of WT HEK and *NPC2*$^{-/-}$ HEK cell lines co-stained with an antibody to LAMP1 (λ_{Ex} = 488 nm, green) and an antibody to TOM20 (λ_{Ex} = 568 nm, red). Nuclei were stained with Hoechst (blue). **e** High content quantification of the late endosomal /lysosomal size performed in WT HEK and *NPC2*$^{-/-}$ HEK stained with an antibody to LAMP1. Each dot of the bar graph indicates the mean value per well of the LAMP1 spot area [µm^2]/cell detected in one well of a 96 well plate. Data are expressed as mean +/− SD. ****$p < 0.0001$, calculated with the Student's T test.

accompanied by other changes of mitochondrial endpoints. Hyperpolarization of mitochondria in the *NPC2*$^{-/-}$ HEK cells might be explained by the V-ATPase working in reverse mode. Fast live-cell imaging techniques can be applied to further understand whether there is any observable movement of protons between the lysosomes and mitochondrial intra-membrane space. Using snap-shot techniques as we have in this study, did not allow for further assessment of this hypothesis. Super resolution dSTORM and EM microscopy data show that there is no overt change in morphology. In addition, high content analysis of the area of the mitochondrial network in WT HEK and *NPC2*$^{-/-}$ HEK cells stained with an antibody against TOM20 indicates that the size of the mitochondrial network in the *NPC2*$^{-/-}$ HEK cells and matched control is similar.

We developed a methodological approach based on three techniques: PLA, super resolution microscopy dSTORM and Transmission Electron Microscopy (TEM). The biochemical assay TOM20-LAMP1 PLA allowed quantification of the incidence of the contacts between the membranes of mitochondria and late endosomes/lysosomes in WT HEK and *NPC2*$^{-/-}$ HEK cells, and robust quantification. Decrease in the cytoplasmic intensity of the TOM20-LAMP1 PLA signal was observed in the *NPC2*$^{-/-}$ HEK cells suggesting that in the absence of the NPC2 protein the contacts between the outer mitochondrial membrane and the lysosomal membrane are reduced. We do not observe significant differences in individual spot area (Supp. Fig. 3c) between the two genotypes which lends confidence that we are able to determine the extent of contact site formation using PLA cytoplasmic intensity. We were able to replicate these findings in several independent experiments (not all reported). In addition, direct visualization of mitochondria-late endosomes/lysosomes contact sites by TEM and super resolution dSTORM corroborated the TOM20-LAMP1 PLA, showing that despite an increase in the lysosomal area and cellular occupancy, the number of contacts between mitochondria and lysosomes is reduced in the *NPC2*$^{-/-}$ HEK cells in comparison to the healthy control. Since membrane contact sites are transient structures with a tethering phase that only lasts for 10–60 s[11], the monitoring of their dynamics by live microscopy would appear to be an ideal method of analysis. However, such an approach would require the ectopic expression of membrane proteins carrying a fluorescent label which most likely would alter the homeostasis of the organellar membrane, as previously reported for other organellar contact sites[7]. We consolidated the high throughput PLA approach with EM and super resolution microscopy thus allowing for different resolution detection and providing the visual proof for the contact sites along with quantification.

The thorough characterization of the *NPC2*$^{-/-}$ HEK cell line conducted in this study demonstrates that *NPC2*$^{-/-}$ HEK is a good model for the study of the organelle dysfunction that are thought to underly the Niemann–Pick disease C Type-2. *NPC2*$^{-/-}$HEK cells recapitulated the lipid dyshomeostasis phenotype of the Niemann–Pick disease C. Notably, we were also able to quantify changes in glucosylsphingosine. The observations of no overt mitochondrial dysfunction or stress induced mitochondrial ROS production (Suppl. Fig. 3; Fig. 4), suggest that the mitochondrial biology is not compromised by the absence of the NPC2 protein, however, there are significant consequences to lysosomal function. The study of mitochondria-late endosomes/lysosomes membrane contact sites revealed that alteration of this equilibrium might be a further pathological process of the disease, as previously found in cellular models of Niemann–Pick C type-1 in which increased extension of the contacts between mitochondria and lysosomes was detected[4]. The PLA data suggest that the NPC2 deficiency results in reduction of the formation of membrane contact sites between mitochondria and late endosomes/lysosomes, in spite of an overall increase in the size of late endosomes/lysosomes. This evidence suggests that the NPC2 protein might indirectly play a role in the formation of mitochondria-late endosomes/lysosomes contact sites. The reconstitution of the protein rescues cholesterol accumulation and lysosomal enlargement. We hypothesize that the deficit in mitochondrial-lysosomal contact sites may result in the loss of an alternative egress pathway, hence affecting lysosomal function.

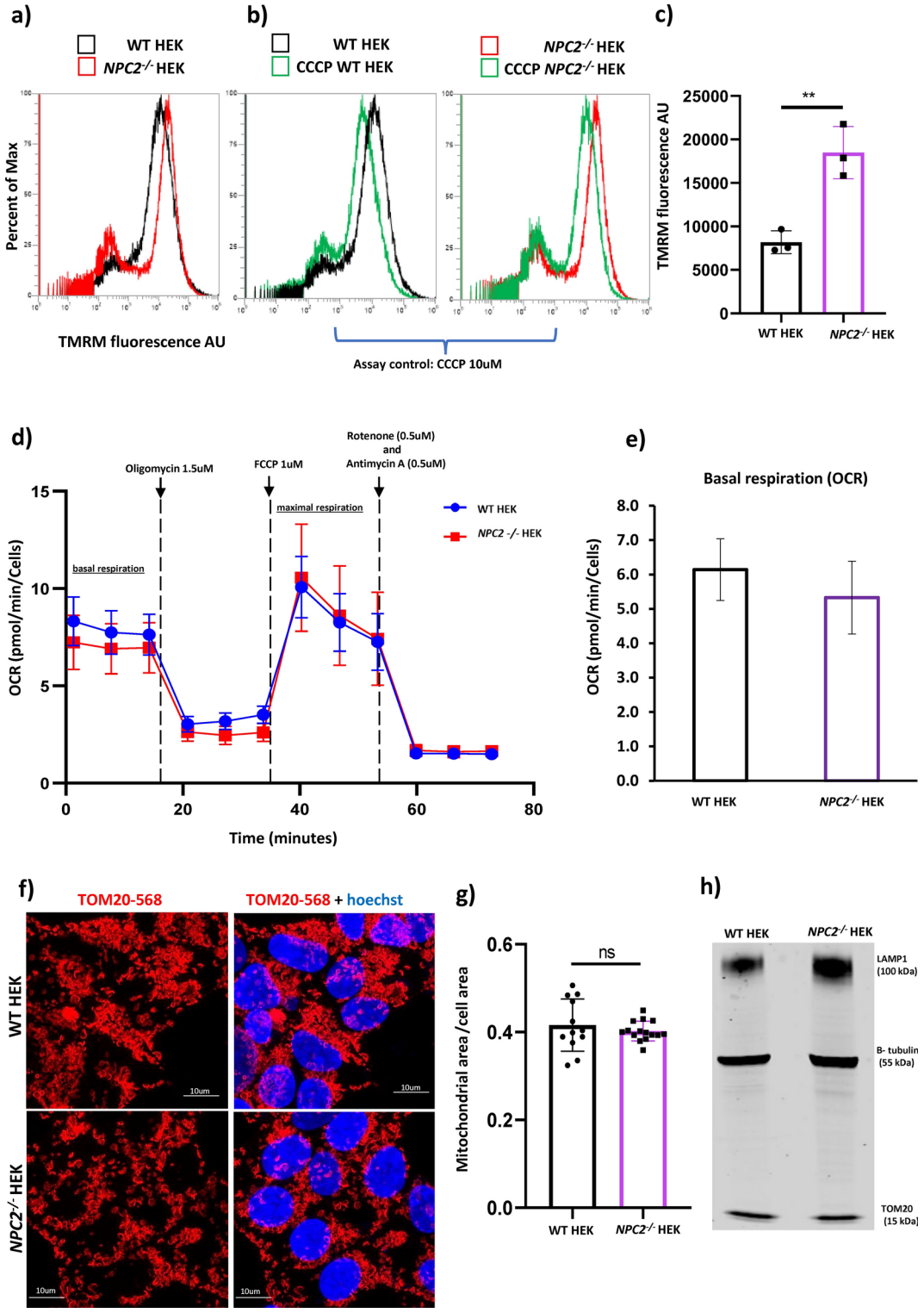

Material and methods

Cell culture

HEKT293 (referred to as wild type WT HEK in the article) and *NPC2*$^{-/-}$ HEK cells were purchased from ATCC and Abcam, respectively. Both cell lines were grown in Dulbecco Modified Eagle's Medium high glucose, supplemented with 10% foetal bovine serum and 1% penicillin–streptomycin at 37 °C in a 5% CO2 incubator.

Super resolution microscopy dSTORM (direct stochastic optical reconstruction microscopy)

WT and *NPC2*$^{-/-}$ HEK cells were seeded on glass coverslips and grown at 37 °C; 5% CO2 for 24 h. On the following day, cells were fixed with 4% PFA for 10 min, permeabilized and blocked with a solution of 2% bovine serum albumin (BSA)-0.1% saponin in PBS 1X for 1 h at RT. Cells were then incubated with primary antibodies against LAMP1 (mouse monoclonal H4A3) and TOM20 overnight at 4 °C. On the following day, secondary

◀**Fig. 4**. Characterization of the mitochondrial function in *NPC2*$^{-/-}$ HEK. **a–d** Tetramethylrhodamine ethyl ester (TMRM, red) assay performed by flow cytometry in WT HEK and *NPC2*$^{-/-}$ HEK cells under basal conditions and after treatment with 10μM carbonyl cyanide-m-chlorophenylhydrazone (CCCP) for 30 min at 37 °C, 5% CO_2. CCCP treatment was used as a positive control for the functionality of the TMRM assay. **a** representative flow cytometry histogram of TMRM experiment carried out in untreated WT HEK and *NPC2*$^{-/-}$ HEK cells. **b** representative flow cytometry histogram of TMRM experiment carried out in WT HEK cells either left untreated or treated with 10 μM CCCP. **c** representative flow cytometry histogram of TMRM experiment carried out in *NPC2*$^{-/-}$ HEK cells either left untreated or treated with 10 μM CCCP. Percent of Max = percentage of cells stained with TMRM. **d** Quantification of the TMRM red fluorescence intensity (λ_{Ex} = 568 nm) detected in WT HEK and *NPC2*$^{-/-}$HEK under basal conditions. AU = arbitrary units. Data were collated from three independent experiments. Each dot the bar graph indicates an independent experiment with data expressed as median of the TMRM fluorescence intensity + /- SEM (Standard Error of the Mean); $^{**}p < 0.01$. *p* value was calculated using the Student's T test. **e** Oxygen Consumption Rate (OCR) determined by Seahorse assay in WT HEK and *NPC2*$^{-/-}$ HEK under basal conditions (basal mitochondrial respiration) and after treatment with pharmacological modulators of the Electron Transport Chain (ETC) such as 1.5 μM oligomycin, 1.0 μM carbonyl cyanide p-trifluoro methoxy phenylhydrazone FCCP (maximal respiration), 0.5 μM rotenone/0.5 μM antimycin. OCR data were expressed as pMol of oxygen consumed per minute, normalized to the number of cells per well of a XF 96 well plate. **f** Representative confocal microscopy images of WT HEK and *NPC2*$^{-/-}$ HEK stained with an antibody against TOM20 (λ_{Ex} = 568nm, red) to label the mitochondrial network. **g** Quantification of the area occupied by the mitochondrial network (TOM20-568nm) detected by high content microscopy and depicted in panel **f**. Data are expressed as μm^2 of TOM20-568 nm per cell. **h** Western blot image displaying the levels of LAMP1 (100kDa) and TOM20 (55 kDa) in WT HEK and *NPC2*$^{-/-}$ HEK. An antibody against β-tubulin was used as gel loading control.

antibodies conjugated with fluorophores, the anti-rabbit Alexa-647 and the anti-mouse Alexa-488 were applied at a dilution of 1:500 for 1 h at RT. dSTORM images were acquired with the ONI (Oxford NanoImager) super resolution microscope, keeping cells in the ONI blinking buffer (100 U glucose oxidase, 2000 U catalase, 55.5 mM glucose and 100 mM cysteamine hydrochloride in sterile PBS) (Oxford Nanoimaging ONI Ltd., UK). Image reconstruction is automatically generated by CODI.

Immunofluorescence

WT and *NPC2*$^{-/-}$ HEK cells were plated on PDL coated 96 well plates and grown at 37 °C; 5% CO2 for 24 h. On the following day, cells were fixed with 4% PFA for 10 min, permeabilized and blocked with a solution of 2% w/v bovine serum albumin (BSA)-0.1% w/v saponin in PBS 1X for 1 h at RT. Cells were then incubated with primary antibodies against LAMP1 (mouse monoclonal H4A3) and TOM20 (rabbit) overnight at 4 °C. On the following day, secondary antibodies conjugated with fluorophores, the anti-rabbit Alexa-647 and the anti-mouse Alexa-488 were applied to the wells at a dilution of 1:500 for 1 h at RT. Fluorescence images were acquired with the Zeiss AXIO Observer Z1 microscope, keeping cells in PBS 1X.

Filipin staining

WT and *NPC2*$^{-/-}$ HEK cells were plated on PDL coated 96 well plates and grown at 37 °C; 5% CO2 for 24 h. On the following day, cells were fixed with PFA 4% for 10 min at room temperature, washed with PBS 1X, incubated with 1 M glycine for 5 min then replaced by 50 ug/ml filipin dissolved 1:100 in the M1 solution protected from light for 1 h at room temperature.

Proximity ligation assay (PLA)

WT HEK and *NPC2*$^{-/-}$ HEK cells were plated on PDL coated 96 well plates and grown at 37 °C; 5% CO2 for 24 h. On the following day, cells were fixed with 4% PFA for 10 min, permeabilized and blocked with a solution of 2% bovine serum albumin (BSA)-0.1% saponin in PBS 1X for 1 h at RT. Cells were then incubated with primary antibodies against LAMP1 (mouse monoclonal H4A3) and TOM20 (rabbit) overnight at 4 °C. Following that, the PLA experiment was carried out applying (using manufacturer's instructions (Duolink PLA fluorescence protocol Sigma-Aldrich). PLA images were acquired using the microscopes: Zeiss Airyscan LSM880 Inverted (The Crick Institute Microscopy unit) and InCell Analyzer 6500.

TMRM assay by flow cytometry for mitochondrial membrane potential (MMP)

Mitochondrial membrane potential was measured using the potentiometric dye tetramethyl rhodamine methyl ester (TMRM; Sigma Aldrich T5428). Cells grown in 6-well plates were treated with the specific compounds of interest, resuspended, transferred into flow cytometry tubes, washed with PBS-1X and incubated with TMRM at a final concentration of 50 nM in complete medium for 30 min at 37 °C. TMRM fluorescence was detected with the Attune NxT Flow Cytometer using a laser $\lambda_{ex.}$ = 568 nm. The mitochondrial uncoupler CCCP 10 μM was used as experimental control to verify that the TMRM assay was performed correctly.

Quantification of sphingolipids by mass spectrometry

WT and NPC2$^{-/-}$ HEK cells were provided as frozen monolayers in 96 well plates as above. Lipid extraction was performed by addition of 150 μL MeOH buffer containing 100 ng/mL d9-sphingomyelin d18:1 (Avanti Polar Lipids LLC., Alabaster, AL) and 10 ng/mL d7-ceramide d16:0 (Avanti), d7-sphingosine d18:1 (Avanti), d3-glucosylceramide d16:0 (Matreya LLC. State College PA) and $^{13}C_6$-glucosylsphingosine d18:1 (Matreya) synthetic

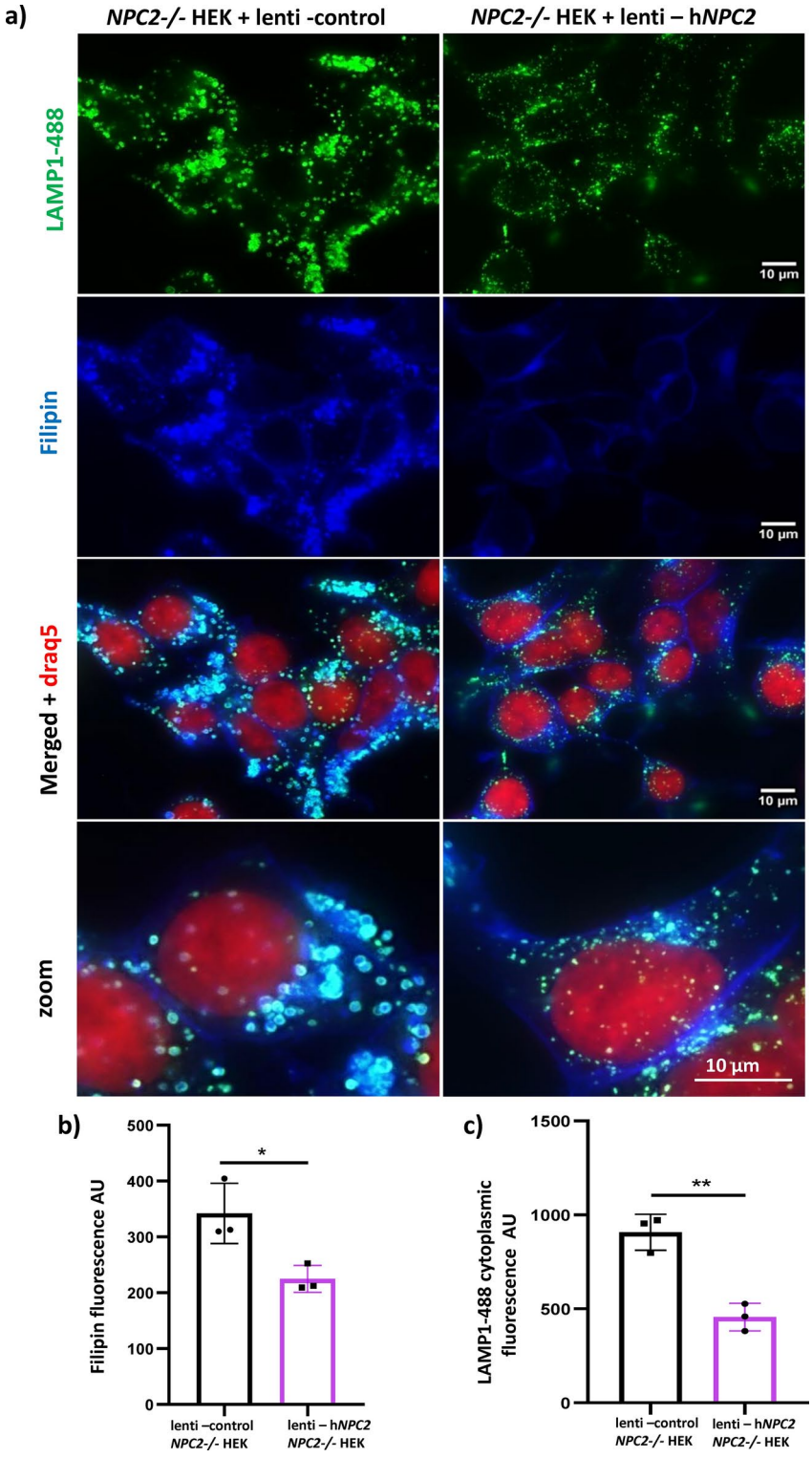

Fig. 5. Reconstitution of the NPC2 protein rescues the levels of unesterified cholesterol in the *NPC2*$^{-/-}$ HEK cells. **a** Representative epifluorescence images of *NPC2*$^{-/-}$ HEK cells transduced with lentiviral control particles or lentiviral particles encoding the human *NPC2* gene (*hNPC2*). Cells were labelled with the fluorescent probe filipin (blue) to mark unesterified cholesterol, DRAQ5-647 (red) to stain the nucleus and an antibody to LAMP1 to mark the late endosomal/lysosomal membrane (green, LAMP1-488). **b, c** Quantification of the filipin fluorescence intensity (unesterified cholesterol) and of the LAMP1-488 cytoplasmic fluorescence intensity (endogenous expression of LAMP1) detected in the experiment described in panel (a). AU = arbitrary units. Data are expressed as mean per well (each dot of the bar graph indicates one well of a 96 well plate) + /− SD. *$p < 0.05$; **$p < 0.01$; p value was calculated with the Student's T test.

standard mix. Plates were capped and shaken for ten minutes at room temperature prior to centrifugation at 1500×g for five minutes to remove cell debris. Lipid-containing supernatant was transferred to 96 well plates for LC–MS/MS analysis.

Quantification of endogenous sphingolipid species was performed by targeted multiple reaction monitoring (MRM) liquid chromatography tandem mass spectrometry. Separation was performed with a HALO HILIC 2.7 mm column (Advanced Materials Technology, Inc., Wilmington, DE) using a Waters Acquity UPLC (Waters Corp., Inc.). Mobile phase A and B consisted of 0.1% formic acid in H2O and 95% acetonitrile, 2.5% MeOH, 2.0% H2O, 0.5% formic acid and 5 mM ammonium formate, respectively. A ten-minute normal phase gradient was sufficient to achieve baseline separation of hexosyl-containing lipids into their respective glucosyl and galactosyl isomeric species. Acquisition was performed with a SciEx 5500 mass spectrometer (SciEx LLC, Framingham, MA) operating in positive ion mode. Absolute quantification was achieved by generating standard curves of selected lipids across each class relative to stable isotopically labelled reference standards. Total glucosylceramide, ceramide, and sphingomyelin concentrations were represented as the sum concentrations of the targeted chain length molecular species.

ROS detection

Reactive oxygen species (ROS) in WT HEK and *NPC2*$^{-/-}$ HEK cells were measured by the fluorescence-based assays CellROX and MitoSOX, which allow detection of ROS levels in the whole cell and within mitochondria, respectively. Treatment of the cells with 15 µM rotenone for 1 h at 37 °C, 5% CO_2 was included as positive control in both assays. WT HEK and *NPC2*$^{-/-}$ HEK cells were seeded in PDL coated 96 well plates and grown overnight in complete medium. On the following day, cells were either left untreated or treated with 15 µM rotenone for 1 h at 37 °C, 5% CO_2. Subsequently, media was replaced with a solution containing either 5 µM CellROX orange or 5 µM MitoSOX, Hoechst and Calcein green in complete medium. After a 20 min incubation at 37 °C, 5% CO_2 images were acquired with the high content microscope InCell Analyzer 6500 and analysed with the Columbus software.

Western blot

Cells were lysed with RIPA buffer and harvested by scraping. Proteins were extracted by sonication and separated by SDS-PAGE in 4–12% (w/v) gradient gels. Each well of the gel was loaded with 20ug of protein. After separation, proteins were transferred to nitrocellulose membranes. Immunoblots were then blocked at room temperature (1 h) and incubated with primary antibodies at 4 °C overnight. Membranes were washed and incubated with secondary antibodies conjugated with fluorophores ($\lambda_{ex.} = 800$ nm and $\lambda_{ex.} = 700$ nm). Images were acquired using the Odyssey-CLX. For quantification, intensity values were normalised to either GAPDH or β-tubulin.

Seahorse assay-oxygen consumption rate (OCR)

WT HEK and *NPC2*$^{-/-}$ HEK cells were plated at a density of 2.5×10^4 cells/well in a PDL coated XF96 cell culture plate (SeaHorse Bioscience) and grown overnight in complete medium at 37 °C, 5% CO_2. On the following day, cells were incubated in XF assay medium supplemented with 5.5 mM D-glucose, 1 mM sodium pyruvate and 2 mM glutamine for 30 min at 37 °C without CO_2. Measurement of the Oxygen Consumption Rate (OCR) was performed using the SeaHorse Bioscience extracellular flux analyser at different time points both at the basal level and during sequential addition of 1.5 µM oligomycin, 1 µM cyanide *p*-trifluoromethoxyphenylhydrazone (FCCP) and 0.5 µM rotenone/antimycin. The OCR values were normalised to the number of cells contained in each well of the XF96 plate.

Lipid peroxidation

Lipid peroxidation in WT HEK and *NPC2*$^{-/-}$ HEK cells was measured using the BODIPY™ 581/591 C11 reagent, Image-iT™ Lipid Peroxidation Kit. WT HEK and *NPC2*$^{-/-}$ HEK cells were seeded in a six-well plate and grown in complete medium at 37 °C, 5% CO_2. On the day of the experiment WT HEK and *NPC2*$^{-/-}$ HEK cells were either left untreated or treated with 100 µM cumene hydroperoxide (CH) for 2 h at 37 °C, 5% CO_2 to induce lipid peroxidation (positive control). After 1.5 h treatment with CH, 10 µM BODIPY 581/591 C11 was added to both groups of cells and incubated for 30 min at 37 °C, 5% CO_2. Subsequently, cells were washed in PBS 1X and analysed with the flow cytometer Attune™ NxT Flow Cytometer. The fluorescence intensity of the BODIPY 581/591 C11 reagent after excitation at $\lambda_{ex.} = 488$ nm was detected at $\lambda_{em.} = 591$ nm (reduced BODIPY 581/591 C11) and at $\lambda_{em.} = 561$ nm (oxidised BODIPY 581/591 C11). Data are reported as percentage of cells expressing the oxidised form of BODIPY 581/591 c11.

Transduction of lentiviral vectors

Lentiviral particles carrying either a construct encoding the human *NPC2* gene (RC200282L3V) or a control construct (PS100064V) were purchased from Origene. *NPC2*$^{-/-}$ HEK cells were transduced with Lenti NPC2 or Lenti control particles at a multiplicity of infection (MOI) of 5 following the manufacturer's instructions. Expression of the transduced NPC2 protein in the *NPC2*$^{-/-}$ HEK cells was verified indirectly by monitoring the levels of unesterified cholesterol (fluorescence intensity of filipin) as well as the size of late endosomes/lysosomes and the expression levels of LAMP1 (immunofluorecence staining of the LAMP1 protein).

Data availability

The datasets used and/or analysed during the current study available from the corresponding author on reasonable request.

Received: 25 March 2024; Accepted: 16 December 2024
Published online: 02 January 2025

References

1. Vanier, M. T. Niemann–Pick disease type C. *Orphanet J. Rare Dis.* **5**, 16. https://doi.org/10.1186/1750-1172-5-16 (2010).
2. Platt, F. M., d'Azzo, A., Davidson, B. L., Neufeld, E. F. & Tifft, C. J. Lysosomal storage diseases. *Nat. Rev. Disease Primers* **4**, 27. https://doi.org/10.1038/s41572-018-0025-4 (2018).
3. Lim, C. Y. et al. ER-lysosome contacts enable cholesterol sensing by mTORC1 and drive aberrant growth signalling in Niemann–Pick type C. *Nat. Cell Biol.* **21**, 1206–1218. https://doi.org/10.1038/s41556-019-0391-5 (2019).
4. Höglinger, D. et al. NPC1 regulates ER contacts with endocytic organelles to mediate cholesterol egress. *Nat. Commun.* **10**, 4276. https://doi.org/10.1038/s41467-019-12152-2 (2019).
5. Kennedy, B. E., Charman, M. & Karten, B. Niemann–Pick Type C2 protein contributes to the transport of endosomal cholesterol to mitochondria without interacting with NPC1. *J. Lipid Res.* **53**, 2632–2642. https://doi.org/10.1194/jlr.M029942 (2012).
6. McCauliff, L. A. et al. Multiple surface regions on the Niemann–Pick C2 protein facilitate intracellular cholesterol transport. *J. Biol. Chem.* **290**, 27321–27331. https://doi.org/10.1074/jbc.M115.667469 (2015).
7. Scorrano, L. et al. Coming together to define membrane contact sites. *Nat. Commun.* **10**, 1287. https://doi.org/10.1038/s41467-019-09253-3 (2019).
8. Peng, W., Wong, Y. C. & Krainc, D. Mitochondria-lysosome contacts regulate mitochondrial Ca(2+) dynamics via lysosomal TRPML1. *Proc. Natl. Acad. Sci. USA* **117**, 19266–19275. https://doi.org/10.1073/pnas.2003236117 (2020).
9. Wilson, E. L. & Metzakopian, E. ER-mitochondria contact sites in neurodegeneration: Genetic screening approaches to investigate novel disease mechanisms. *Cell Death Differ.* **28**, 1804–1821. https://doi.org/10.1038/s41418-020-00705-8 (2021).
10. Wong, Y. C., Kim, S., Peng, W. & Krainc, D. Regulation and function of mitochondria-lysosome membrane contact sites in cellular homeostasis. *Trends. Cell Biol.* **29**, 500–513. https://doi.org/10.1016/j.tcb.2019.02.004 (2019).
11. Wong, Y. C., Ysselstein, D. & Krainc, D. Mitochondria–lysosome contacts regulate mitochondrial fission via RAB7 GTP hydrolysis. *Nature* **554**, 382–386. https://doi.org/10.1038/nature25486 (2018).
12. Kim, S., Wong, Y. C., Gao, F. & Krainc, D. Dysregulation of mitochondria-lysosome contacts by GBA1 dysfunction in dopaminergic neuronal models of Parkinson's disease. *Nat. Commun.* **12**, 1807. https://doi.org/10.1038/s41467-021-22113-3 (2021).
13. Cantarero, L. et al. Mitochondria-lysosome membrane contacts are defective in GDAP1-related Charcot-Marie-Tooth disease. *Hum. Mol. Genet.* **29**, 3589–3605. https://doi.org/10.1093/hmg/ddaa243 (2021).
14. Kim, J. & Bai, H. Peroxisomal stress response and inter-organelle communication in cellular homeostasis and aging. *Antioxidants (Basel)* https://doi.org/10.3390/antiox11020192 (2022).
15. Cisneros, J., Belton, T. B., Shum, G. C., Molakal, C. G. & Wong, Y. C. Mitochondria-lysosome contact site dynamics and misregulation in neurodegenerative diseases. *Trends. Neurosci.* **45**, 312–322. https://doi.org/10.1016/j.tins.2022.01.005 (2022).
16. Onoue, K. et al. Fis1 acts as a mitochondrial recruitment factor for TBC1D15 that is involved in regulation of mitochondrial morphology. *J. Cell Sci.* **126**, 176–185. https://doi.org/10.1242/jcs.111211 (2013).
17. Pankiv, S. et al. FYCO1 is a Rab7 effector that binds to LC3 and PI3P to mediate microtubule plus end-directed vesicle transport. *J. Cell Biol.* **188**, 253–269. https://doi.org/10.1083/jcb.200907015 (2010).
18. Elustondo, P., Martin, L. A. & Karten, B. Mitochondrial cholesterol import. *Biochim. Biophys. Acta Mol. Cell Biol. Lipids* **90–101**, 2017. https://doi.org/10.1016/j.bbalip.2016.08.012 (1862).
19. Charman, M., Kennedy, B. E., Osborne, N. & Karten, B. MLN64 mediates egress of cholesterol from endosomes to mitochondria in the absence of functional Niemann–Pick Type C1 protein. *J. Lipid. Res.* **51**, 1023–1034. https://doi.org/10.1194/jlr.M002345 (2010).
20. Juhl, A. D. et al. Quantitative imaging of membrane contact sites for sterol transfer between endo-lysosomes and mitochondria in living cells. *Sci. Rep.* **11**, 8927. https://doi.org/10.1038/s41598-021-87876-7 (2021).
21. Kwon, H. J. et al. Structure of N-terminal domain of NPC1 reveals distinct subdomains for binding and transfer of cholesterol. *Cell* **137**, 1213–1224. https://doi.org/10.1016/j.cell.2009.03.049 (2009).
22. Pfeffer, S. R. NPC intracellular cholesterol transporter 1 (NPC1)-mediated cholesterol export from lysosomes. *J. Biol. Chem.* **294**, 1706–1709. https://doi.org/10.1074/jbc.TM118.004165 (2019).
23. Li, X., Saha, P., Li, J., Blobel, G. & Pfeffer, S. R. Clues to the mechanism of cholesterol transfer from the structure of NPC1 middle lumenal domain bound to NPC2. *Proc. Natl. Acad. Sci. U S A* **113**, 10079–10084. https://doi.org/10.1073/pnas.1611956113 (2016).
24. Xu, Z., Farver, W., Kodukula, S. & Storch, J. Regulation of sterol transport between membranes and NPC2. *Biochemistry* **47**, 11134–11143. https://doi.org/10.1021/bi801328u (2008).
25. Cheruku, S. R., Xu, Z., Dutia, R., Lobel, P. & Storch, J. Mechanism of cholesterol transfer from the Niemann–Pick type C2 protein to model membranes supports a role in lysosomal cholesterol transport. *J. Biol. Chem.* **281**, 31594–31604. https://doi.org/10.1074/jbc.M602765200 (2006).
26. Bruno, F., Camuso, S., Capuozzo, E. & Canterini, S. the antifungal antibiotic filipin as a diagnostic tool of cholesterol alterations in lysosomal storage diseases and neurodegenerative disorders. *Antibiotics (Basel).* https://doi.org/10.3390/antibiotics12010122 (2023).
27. Rosenbaum, A. I., Zhang, G., Warren, J. D. & Maxfield, F. R. Endocytosis of beta-cyclodextrins is responsible for cholesterol reduction in Niemann–Pick type C mutant cells. *Proc. Natl. Acad. Sci.* **107**, 5477–5482. https://doi.org/10.1073/pnas.0914309107 (2010).
28. Alam, M. S. Proximity Ligation Assay (PLA). *Curr. Protoc. Immunol.* **123**, e58. https://doi.org/10.1002/cpim.58 (2018).
29. Hegazy, M. et al. Proximity ligation assay for detecting protein-protein interactions and protein modifications in cells and tissues in situ. *Curr. Protoc. Cell Biol.* **89**, e115. https://doi.org/10.1002/cpcb.115 (2020).
30. Las Heras, M. et al. Understanding the phenotypic variability in Niemann–Pick disease type C (NPC): A need for precision medicine. *NPJ Genomic. Med.* **8**, 21. https://doi.org/10.1038/s41525-023-00365-w (2023).
31. Wong, Y. C., Peng, W. & Krainc, D. Lysosomal regulation of inter-mitochondrial contact fate and motility in charcot-marie-tooth type 2. *Dev. Cell* **50**, 339-354.e334. https://doi.org/10.1016/j.devcel.2019.05.033 (2019).
32. Peng, W., Schröder, L. F., Song, P., Wong, Y. C. & Krainc, D. Parkin regulates amino acid homeostasis at mitochondria-lysosome (M/L) contact sites in Parkinson's disease. *Sci. Adv.* **9**, eadh3347. https://doi.org/10.1126/sciadv.adh3347 (2023).
33. Höglinger, D. et al. Intracellular sphingosine releases calcium from lysosomes. *Elife.* https://doi.org/10.7554/eLife.10616 (2015).
34. Srikanth, M. P. et al. Elevated Glucosylsphingosine in gaucher disease induced pluripotent stem cell neurons deregulates lysosomal compartment through mammalian target of rapamycin complex 1. *Stem Cells Trans. Med.* **10**, 1081–1094. https://doi.org/10.1002/sctm.20-0386 (2021).
35. Arkadir, D. et al. Glucosylsphingosine is a reliable response biomarker in Gaucher disease. *Am. J. Hematol.* **93**, E140-e142. https://doi.org/10.1002/ajh.25074 (2018).

Author contributions

RD and RP wrote the main manuscript text and prepared figures LY and NH prepared figures on the LC–MS lipid measurements MH helped with preparation of manuscript and microscopy support JB helped with prepa-

ration of manuscript and intellectual input into project All authors reviewed the manuscript.

Declarations

Competing interests

Authors are employees of Merck Sharp & Dohme Corp., a subsidiary of Merck & Co., Inc., Kenilworth, NJ, USA and may hold stocks and/or stock options in Merck & Co., Inc., Kenilworth, NJ, USA.

Additional information

Supplementary Information The online version contains supplementary material available at https://doi.org/10.1038/s41598-024-83460-x.

Correspondence and requests for materials should be addressed to R.D.

Reprints and permissions information is available at www.nature.com/reprints.

Publisher's note Springer Nature remains neutral with regard to jurisdictional claims in published maps and institutional affiliations.